Bulletin of Mathematical Biology (2023) 85:57
https://doi.org/10.1007/s11538-023-01143-6

Society for Mathematical Biology

ORIGINAL ARTICLE

Autoregulation of Transcription and Translation: A Qualitative Analysis

Philip J. Murray[1]

Received: 29 June 2022 / Accepted: 9 March 2023 / Published online: 26 May 2023

Abstract
The regulation of both mRNA transcription and translation by down-stream gene products allows for a range of rich dynamical behaviours (e.g. homeostatic, oscillatory, excitability and intermittent solutions). Here, qualitative analysis is applied to an existing model of a gene regulatory network in which a protein dimer inhibits its own transcription and upregulates its own translation rate. It is demonstrated that the model possesses a unique steady state, conditions are derived under which limit cycle solutions arise and estimates are provided for the oscillator period in the limiting case of a relaxation oscillator. The analysis demonstrates that oscillations can arise only if mRNA is more stable than protein and the effect of nonlinear translation inhibition is sufficiently strong. Moreover, it is shown that the oscillation period can vary non-monotonically with transcription rate. Thus the proposed framework can provide an explanation for observed species-specific dependency of segmentation clock period on Notch signalling activity. Finally, this study facilitates the application of the proposed model to more general biological settings where post transcriptional regulation effects are likely important.

Keywords Translation · Molecular oscillator · Relaxation oscillator · Transcription · Notch signalling

1 Introduction

The design principles that underpin oscillations in biological systems are naturally described using mathematical approaches (Alon 2019; Winfree 2001; Novák and Tyson 2008; Tyson and Novák 2010). There are now numerous well established models across a range of cellular oscillators [e.g. cell cycle, circadian cycle, cardiac cycle, gly-

✉ Philip J. Murray
pmurray@dundee.ac.uk

[1] University of Dundee, Dundee, UK

colysis (Sel'Kov 1968), NFκb (Gonze and Abou-Jaoudé 2013), p. 53, (Geva-Zatorsky et al. 2006)].

A conserved principle of the Hes/Her oscillator, now known to be present in many different cell types (Kageyama et al. 2007), is that dimerised members of the basic Helix-loop-helix family of transcription factors (e.g. Hes7, Hes1, Her7) inhibit their own transcription and therefore provide a negative feedback loop. The Notch signalling pathway, which plays a crucial role in embryo development, tissue homeostasis (van Es et al. 2005) and cancer (Mollen et al. 2018; Allenspach et al. 2002; Siebel and Lendahl 2017), can activate the transcription of Hes/Her genes. During canonical *in trans* Notch signalling, a Notch ligand in a signalling cell activates a Notch receptor in a neighbour, resulting in the release of the Notch intracellular domain (NICD) in the receiver, which regulates the transcription of Notch target genes. As at least in some biological contexts, such as the segmentation clock, Notch receptors are themselves a target of Notch signalling and levels of the Delta ligand can be regulated by Hes7 (Bone et al. 2014), the study of Notch signalling is a highly nonlinear problem.

Upon inclusion of time delays that represent processes such as transcription, splicing, transport and translation, it has been shown that negative feedback of transcription is sufficient to give rise to oscillations (Lewis 2003; Monk 2003). Moreover, it has been shown that the spatial diffusion of mRNA and protein is a sufficient mechanism to give rise to oscillations in a negative feedback system (Sturrock et al. 2011; Chaplain et al. 2015). Each of the above models makes the assumption that the translation of mRNA is linear, and thus unregulated.

Recent experimental observations challenge, at least in specific biological contexts, many existing models of the Notch signalling pathway. Oates and coworkers have demonstrated that when levels of Delta ligand are increased in presomitic mesoderm (PSM) cells, the tissue scale oscillator period decreases (Liao et al. 2016). Moreover, when levels of Notch signalling are reduced via treatment with the gamma secretase inhibitor DAPT, which blocks the release of NICD, the tissue scale oscillator period increases (Herrgen et al. 2010). Thus in the zebrafish embryo, the tissue-scale oscillator period appears to be anticorrelated with Notch signalling activity. In contrast, Dale and coworkers have demonstrated that when mouse and chick embryos are exposed to pharmacological treatments that increase levels of NICD, the tissue scale period increases (Wiedermann et al. 2015). Notably, a prediction of the delayed feedback models of the Her oscillator (Lewis 2003) is that the clock period has a strong dependence on the mRNA and protein half lives and time delays but not on transcription or translation rates (Lewis 2003).

Suggestions that mouse PSM tissue behaves like an excitable medium are also difficult to reconcile with delayed negative feedback models of the Notch signalling pathway. It has been identified that NICD is necessary for the oscillations of the segmentation clock in the presence of mechanosensitive Yap signalling (Hubaud et al. 2017). However, when Yap signalling is pharmacologically inhibited, oscillations could still proceed in the absence of Notch signalling. The presence of a Yap-signalling dependent threshold led the authors to conclude that the system under study behaved like an excitable medium. However, there is currently no molecular scale model of Hes7 dynamics that can account for such excitability.

In the Hes1 oscillator in mouse neural cells, the miRNA mir-9 has been identified (Bonev et al. 2012; Goodfellow et al. 2014) as a part of a double negative (i.e. positive) feedback loop in which mir-9 is under the same transcriptional control as the Hes1 gene but serves to inhibit translation. Together, these observations indicate that, at least in some specific biological contexts, the negative feedback model of the Notch signalling pathway is incomplete.

We recently developed an ordinary differential equation model that postulates that an intermediary, X, that is under the same transcriptional control as mRNA, M, inhibits translation [see Fig. 1a (Murray et al. 2021)]. Assuming quasi equilibrium for X, these assumptions introduce a positive feedback loop such that the translation rate increases sigmoidally with protein concentration (see Fig. 1b). Letting $M = M(t)$ and $P = P(t)$ represent the concentrations of mRNA and its corresponding protein at time t, respectively, the governing ODEs are

$$\begin{aligned}\frac{\mathrm{d}M}{\mathrm{d}t} &= \frac{k_1}{1+\left(\frac{P}{P_0}\right)^2} - k_2 M,\\ \frac{\mathrm{d}P}{\mathrm{d}t} &= M\left(k_3 + \frac{k_4}{1+\frac{\alpha}{X_0}\frac{1}{\left(1+\left(\frac{P}{P_0}\right)^2\right)}}\right) - k_5 P,\end{aligned} \tag{1}$$

where k_1 is the maximal transcription rate, P_0 is the protein concentration at which transcription rate is half maximal, k_2 is the mRNA degradation rate, k_3 is the basal translation rate, k_4 is a translation rate that is inhibited by X, α is maximal level of X at steady state, X_0 is an IC50 constant for translational activation and k_5 is the protein degradation rate.

Using parameter values based on the zebrafish Her oscillator, it was shown, using numerical exploration, that Eq. (1) can possess excitable, homeostatic or oscillatory solutions (Murray et al. 2021). Using numerical continuation it was shown that Eq. (1) possess a subcritical Hopf bifurcation such that, in a particular region of parameter space, unstable limit cycle, stable limit cycle and stable steady state solutions coexist. In this case a stochastic implementation of the model is capable of exhibiting intermittent oscillations whereby noise switches the dynamics between a stable limit cycle and a stable steady state. Finally, it was shown that the oscillator period has, for the considered parameters, an inverse dependence on the transcription rate k_1. Hence the proposal that regulation of translation, as well as transcription, rates provides a minimal framework that yields phenomena consistent with recent experimental observations.

Whilst the previous work used numerical solutions to demonstrate interesting model behaviours, a qualitative analysis of the model behaviour is required in order that the model can be explored in more general biological contexts. Here this issue is addressed. The approach taken allows one to relate different Notch signalling behaviours in species-specific contexts (e.g. in which reaction rates may differ significantly). Parameter regimes are identified in which one expects to find different modes of behaviour

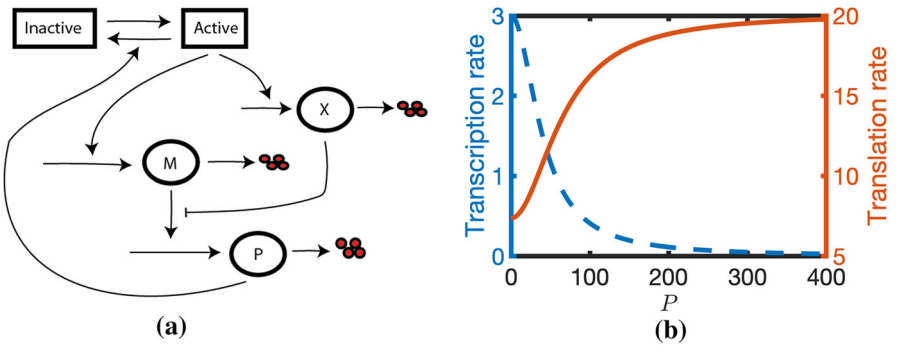

Fig. 1 **a** A schematic illustration of the model. Active/Inactive denote transcriptional states of gene. mRNA is transcribed when the gene is active and degrades. Protein is translated from mRNA and degrades. **b** Translation and transcription rates plotted against protein levels, P

(e.g. excitability, homeostasis, oscillations). Finally, an estimate is derived for the oscillator period and amplitude in the relaxation oscillator limit.

2 Nondimensionalisation

Consider the dimensionless variables

$$m = \frac{M}{\tilde{M}}, \quad p = \frac{P}{\tilde{P}} \quad \text{and} \quad \tau = \frac{t}{\tilde{T}}.$$

Letting

$$\tilde{M} = \frac{k_5 P_0}{k_3} \frac{\left(1 + \frac{\alpha}{X_0}\right)^{\frac{1}{2}}}{\left(1 + \frac{k_4}{k_3}\right)}, \quad \tilde{P} = P_0 \left(1 + \frac{\alpha}{X_0}\right)^{\frac{1}{2}} \quad \text{and} \quad \tilde{T} = \frac{1}{k_5},$$

Equation (1) transforms to the nondimensional form

$$\begin{aligned} \frac{\mathrm{d}m}{\mathrm{d}\tau} &= \frac{\eta_1}{1 + \frac{p^2}{\eta_2}} - \eta_3 m, \\ \frac{\mathrm{d}p}{\mathrm{d}\tau} &= m \frac{(\eta_4 + p^2)}{1 + p^2} - p, \end{aligned} \tag{2}$$

where

$$\eta_1 = \frac{k_1(k_3 + k_4)}{k_5^2 P_0 \sqrt{1 + \frac{\alpha}{X_0}}}, \quad \eta_2 = \frac{1}{1 + \frac{\alpha}{X_0}}, \quad \eta_3 = \frac{k_2}{k_5}, \quad \eta_4 = \frac{1 + \frac{k_4}{k_3} + \frac{\alpha}{X_0}}{\left(1 + \frac{k_4}{k_3}\right)\left(1 + \frac{\alpha}{X_0}\right)}. \tag{3}$$

Table 1 A table of dimensionless parameter values

Parameter	Description	Value
η_1	mRNA transcription	0.76
η_2	Transcriptional inhibition IC50	0.008
η_3	mRNA degradation	0.02
η_4	Translation	0.01

Note that time has been nondimensionalised on the protein degradation timescale, the parameter η_4 represents the strength of the sigmoidal effect on translation rate and that η_3 is the ratio of mRNA to protein degradation rates. See Table 1 for typical values.

3 Nullclines

The p nullcline, given by

$$\bar{m}_2(p) = \frac{p(1+p^2)}{\eta_4 + p^2}, \tag{4}$$

has two distinct real positive turning points if the condition

$$\eta_4 < \frac{1}{9}$$

holds (see Appendix A). The turning points occur at approximately

$$(p_1, m_1) = \left(\sqrt{\eta_4}, \frac{1}{2\sqrt{\eta_4}}\right),$$

and

$$(p_2, m_2) = (1, 2),$$

(see Fig. 2). Note that the condition $\eta_4 < 1/9$ implies that $m_1 > m_2$ and $p_1 < p_2$. Hence (p_1, m_1) is a local maximum and (p_2, m_2) is a local minimum.

The m nullcline, given by

$$\bar{m}_1(p) = \frac{\eta_1}{\eta_3} \frac{1}{1 + \frac{p^2}{\eta_2}}, \tag{5}$$

is monotonically decreasing for $p > 0$ with an IC50 at $p = \sqrt{\eta_2}$ and local maximum of η_1/η_3. In order that nondimensional parameters correspond to positive dimensional parameters, the condition

$$\eta_2 < \eta_4$$

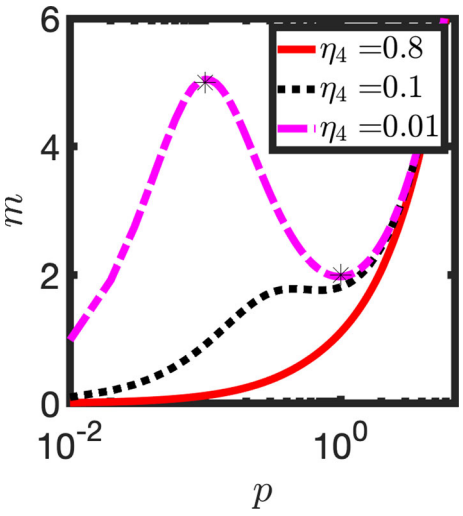

Fig. 2 The p nullcline [see Eq. (4)] is plotted against p for different values of the parameter η_4. Markers denote coordinates of the extrema. Other parameters as in Table 1

must hold (see Appendix A). Hence the IC50 for transcriptional inhibition must be at least an order of magnitude less than the IC50 for the translational switch (which occurs at approximately $p = 1$).

4 Steady State Analysis

Suppose that (m^*, p^*) is a steady state of Eq. (2). Upon elimination of m^*, p^* satisfies the fifth order polynomial

$$h(p^*) = p^{*5} + p^{*3}(\eta_2 + 1) - p^{*2}\frac{\eta_1\eta_2}{\eta_3} + \eta_2 p^* - \frac{\eta_1\eta_2\eta_4}{\eta_3} = 0. \tag{6}$$

Recalling that $\eta_j > 0 \ \forall \ j$, application of Descartes' rule of signs implies that there are at most three real positive solutions of Eq. (6). Moreover, as

$$h(0) = -\frac{\eta_1\eta_2\eta_4}{\eta_3} < 0 \quad \text{and} \quad h(p^*) \to \infty \quad \text{as} \quad p^* \to \infty,$$

Equation (6) must have at least one real positive solution. Applying a graphical method (see Appendix B) it can be shown that, for biologically relevant parameter values, Eq. (6) possesses exactly one solution. This result precludes the possibility of bistability.

5 Linear Stability Analysis

After substitution for the identity

$$m^* = \frac{p^*(1+p^{*2})}{\eta_4 + p^{*2}},$$

the Jacobian matrix of equations (2) takes the form

$$J = \begin{pmatrix} -\eta_3 & -2\frac{\eta_1}{\eta_2}\dfrac{p}{\left(1+\frac{p^2}{\eta_2}\right)^2} \\ \dfrac{\eta_4+p^2}{1+p^2} & -\frac{p^4+p^2(3\eta_4-1)+\eta_4}{(\eta_4+p^2)(1+p^2)} \end{pmatrix}_{(m^*,p^*)}. \tag{7}$$

Given that Eq. (3) possesses a unique steady state in the positive quadrant, the sign structure of the Jacobian matrix is given by

$$\begin{pmatrix} - & - \\ + & \pm \end{pmatrix}. \tag{8}$$

5.1 Intersections on the Left and Right Branches are Linearly Stable

Negativity of the (2, 2) entry of the Jacobian matrix implies that

$$p^{*4} + p^{*2}(3\eta_4 - 1) + \eta_4 > 0, \tag{9}$$

the left-hand side of which has previously been used to compute the turning points of the p nullcline (labelled as p_1 and p_2, see Eq. (19) in Appendix A). Hence when $p^* < p_1$ or $p^* > p_2$, such that the intersection between the m and p nullclines occurs on the left- or right-most branches of the p nullcline, respectively, the (2, 2) entry of the Jacobian matrix is negative and the steady state of Eq. (2) is therefore linearly stable.

5.1.1 The Steady State on the Central Branch of the *p* Nullcline is Conditionally Linearly Stable

The determinant of the Jacobian matrix is positive definite (see Appendix C). Hence the unique steady state of Eq. (2) is linearly unstable if and only if

$$\mathrm{tr}(J) = -\eta_3 - \frac{p^4 + p^2(3\eta_4 - 1) + \eta_4}{(\eta_4 + p^2)(1+p^2)} > 0. \tag{10}$$

This inequality can be expressed as

$$p^{*4}(1+\eta_3) - p^{*2}\left(1 - 3\eta_4 - \eta_3(1+\eta_4)\right) + \eta_4(1+\eta_3) < 0, \tag{11}$$

with the boundaries of the solution interval given by

$$p_c = \pm \left(\frac{1 - 3\eta_4 - \eta_3(1+\eta_4) \pm \left((1 - 3\eta_4 - \eta_3(1+\eta_4))^2 - 4\eta_4(1+\eta_3)^2\right)^{\frac{1}{2}}}{2(1+\eta_3)} \right)^{\frac{1}{2}}. \tag{12}$$

For a real and positive solution interval it is therefore required that

$$1 - 3\eta_4 - \eta_3(1+\eta_4) > 0 \implies \eta_3 < \frac{1-3\eta_4}{1+\eta_4} \implies \eta_3 < 1,$$

and

$$\left((1 - 3\eta_4 - \eta_3(1+\eta_4))^2 - 4\eta_4(1+\eta_3)^2\right) > 0,$$

which can, upon rearrangement, be written as

$$\eta_4 < \left(\frac{\eta_3 - 1}{3+\eta_3}\right)^2.$$

Considering the case where $\eta_3 < 1$, a necessary (but not sufficient) condition for instability of the steady state is

$$\eta_3 < \frac{1 - 3\sqrt{\eta_4}}{1+\sqrt{\eta_4}}. \tag{13}$$

In summary, when the conditions

$$\eta_2 < \eta_4 < \frac{1}{9}, \quad \eta_3 < \frac{1 - 3\sqrt{\eta_4}}{1+\sqrt{\eta_4}} \tag{14}$$

hold, there is always a real interval of p^* within which $\mathrm{tr}(A)$ is positive and the steady state is therefore linearly unstable. As p^* is a monotonically increasing function of η_1 (see Appendix B) a corresponding interval of the parameter η_1 can always be found such that the unique steady state (p^*, m^*) is linearly unstable. This result implies that too little or too much basal transcription (i.e. k_1) will result in the disappearance of oscillatory solutions.

6 Limit Cycle Solutions

A confined set can be defined for Eq. (2) (see Appendix D). Given the existence of a unique steady state, the Poincare Bendixson theorem can be applied in order to show that there is an interval of the parameter η_1 for which Eq. (2) have limit cycle solutions.

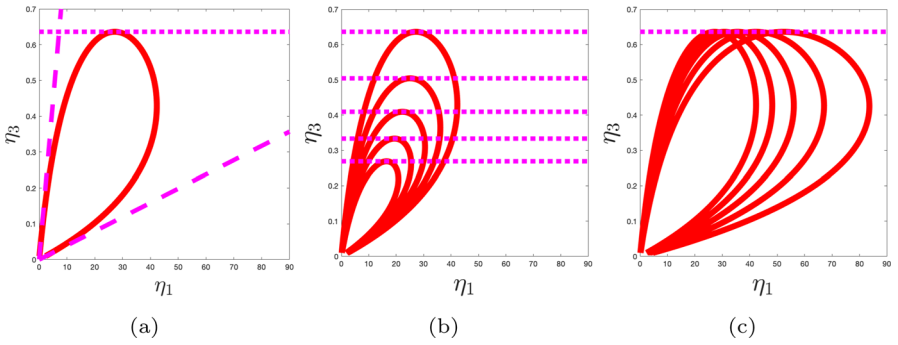

Fig. 3 Planar projections of Hopf bifurcation surface. **a** A family of Hopf bifurcation points are represented by the red curve in the $\eta_1 - \eta_3$ plane. The dotted horizontal line represents condition (14). Dashed lines represent equations (15). **b** Each loop in the $\eta_1 - \eta_3$ plane represents a family of Hopf bifurcations at a different fixed value of the parameter η_4. **c** Each loop in the $\eta_1 - \eta_3$ plane represents a family of Hopf bifurcations at a different fixed value of the parameter η_2. Parameter values as in Table 1 unless otherwise stated (Color figure online)

6.1 Numerical Continuation

Numerical continuation was performed (Dankowicz and Schilder 2013) to confirm the presence of a family of Hopf bifurcations in the $\eta_1 - \eta_3$ plane (see Fig. 3a). These numerical results indicate that, given that inequalities (14) hold, one can find an interval of the parameter η_1 in which there are limit cycle solutions. Note that the derived upper bound on η_3, given by inequality (13), is consistent with the upper bound estimated using continuation. Moreover, by imposing the conditions

$$m_2(p_1) > m_1(p_1) \quad \text{and} \quad m_2(p_2) < m_2(p_1),$$

such that the nullclines intersect in the middle branch of the p nullcline, a necessary condition for limit cycle solutions is

$$\frac{1+\dfrac{\eta_4}{\eta_2}}{2\sqrt{\eta_4}} < \frac{\eta_1}{\eta_3} < 2\left(1+\frac{1}{\eta_2}\right). \tag{15}$$

These bounds are presented in Fig. 3a. In Fig. 3b, c the Hopf bifurcation surface is projected onto the $\eta_1 - \eta_3$ plane for different values of η_4 and η_2, respectively. Note that, as expected, the maximum value of η_3 for which oscillatory solutions are possible varies with the parameter η_4 (see Fig. 3b) but not η_2 (see Fig. 3c).

Numerical continuation also indicates that the classification of the Hopf bifurcation that arises for smaller η_1 is dependent on the parameter η_3. For larger η_3, there are two supercritical Hopf bifurcations. Here the amplitude of oscillations increases close to both bifurcation points (see Fig. 4a–c). However, for smaller η_3 the Hopf bifurcation is subcritical and one observes the emergence of a saddle node bifurcation of the limit cycle. In this case there is an interval of the parameter η_1 in which there is an unstable limit cycle, a stable steady state and a stable limit cycle (see Fig. 4d–f). In

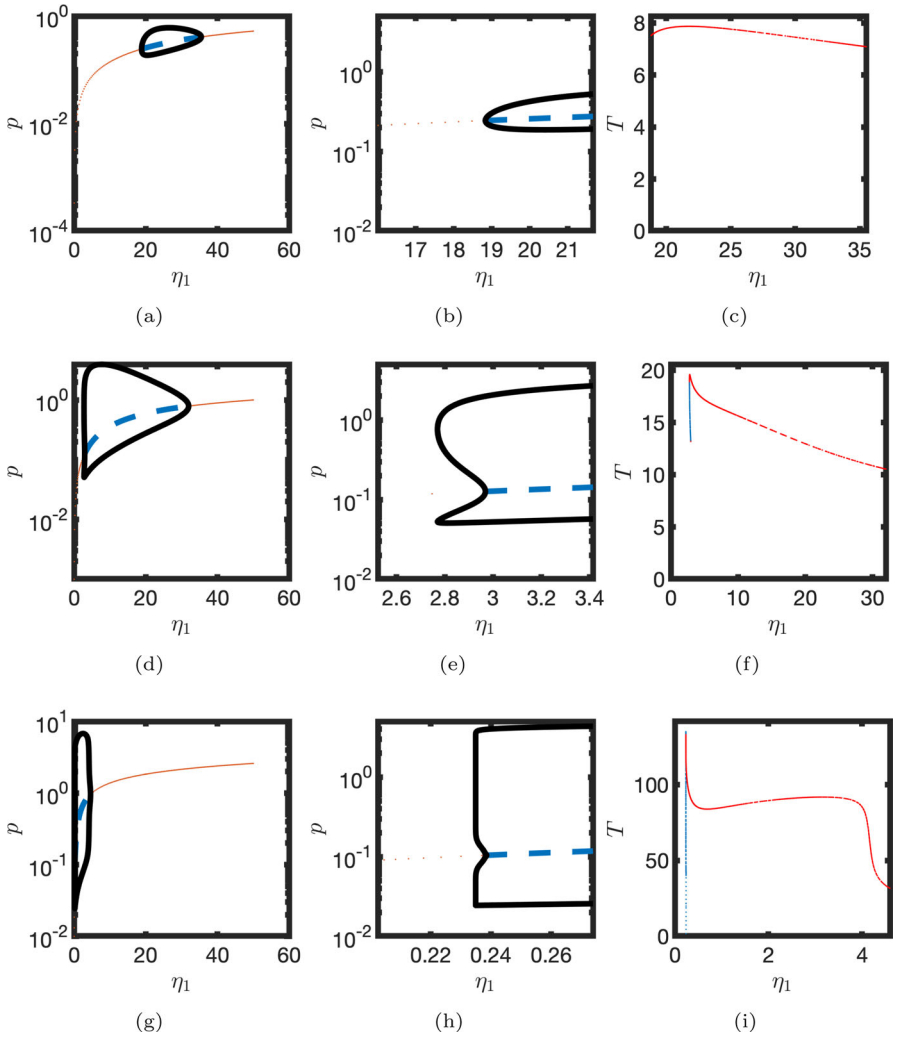

Fig. 4 Hopf bifurcations for different values of the parameter η_3. Top row, $\eta_3 = 0.6$. Middle row, $\eta_3 = 0.2$. Bottom row, $\eta_3 = 0.02$. Left column, steady state levels of protein, p, plotted against η_1 (blue dashed line, unstable; red line, stable). Solid black lines represent maxima/minima of the p component of limit cycle solutions. Middle column—inset for left column. Right column—oscillator period is plotted against η_1. Red markers—stable limit cycle. Blue markers—unstable limit cycle. Parameters as in Table 1 unless otherwise stated (Color figure online)

the limiting case, where both η_1 and η_3 are small, the time scale of mRNA production and degradation are relatively long and the system behaves like a relaxation oscillator (see Fig. 4g–i). Notably, the dependence of the oscillator period on the parameter η_1 is in general not monotonic.

6.2 Period and Amplitude Estimate in the Relaxation Oscillator Limit

Under the assumption that inequalities (14) hold, an estimate for the oscillator period can be derived. Consider the case where the time scale of mRNA transcription and degradation is much longer than that of translation. After applying a fast-slow time scale analysis, where the mRNA is the slow variable, the limit cycle is approximated by a trajectory ABCD (see Fig. 5b) with coordinates

$$\begin{aligned}&(m_A, p_A) = (2 - 2\eta_4, 2\eta_4), \quad (m_B, p_B) = \left(\frac{1}{2\sqrt{\eta_4}}(1 + \eta_4), \sqrt{\eta_4}(1 + 2\eta_4)\right),\\ &(m_C, p_C) = \left(\frac{1}{2\sqrt{\eta_4}}(1 + \eta_4), \frac{1}{2\sqrt{\eta_4}}(1 + \eta_4)\right) \quad \text{and} \quad (m_D, p_D) = (2 - 2\eta_4, 1 - 2\eta_4).\end{aligned} \tag{16}$$

A lower bound for the oscillator period (see Appendix E) is given by

$$T \sim T_{AB} + T_{CD} = \frac{1}{2\eta_1\sqrt{\eta_4}} + \frac{1}{\eta_3}\ln\left(\frac{1}{4\sqrt{\eta_4}}\right). \tag{17}$$

Thus in the relaxation oscillator limit the period varies inversely with the parameter η_1. The amplitudes of protein and mRNA oscillation are approximated by

$$A_P = p_C - p_A = \frac{1}{2\sqrt{\eta_4}} - 2\eta_4 \sim \frac{1}{2\sqrt{\eta_4}} \quad \text{and} \quad A_M = m_B - m_A \sim \frac{1}{2\sqrt{\eta_4}},$$

respectively. In Fig. 5c–f the derived estimates for the oscillator period are compared with numerical estimates. It is noted that as the oscillator is made less stiff, a correction is needed to Eq. (17) that accounts for time spent close to the local maximum of the p nullcline (see Appendix E). In this case the estimate of the oscillator period no longer depends monotonically on the parameter η_1.

6.3 Dimensional Parameters

6.3.1 The Oscillatory Region

Returning to dimensional parameters, the condition $\eta_4 < 1/9$ (see Appendix A) implies that

$$\frac{k_4}{k_3} > 8 \quad \text{and} \quad \frac{\alpha}{x_0} > 8.$$

Thus for the p nullcline to have two turning points there must be a significant upregulation of the net translation rate and the maximal level of X must be much larger than the IC50 for the upregulation of the translation rate. Upon expansion in the small

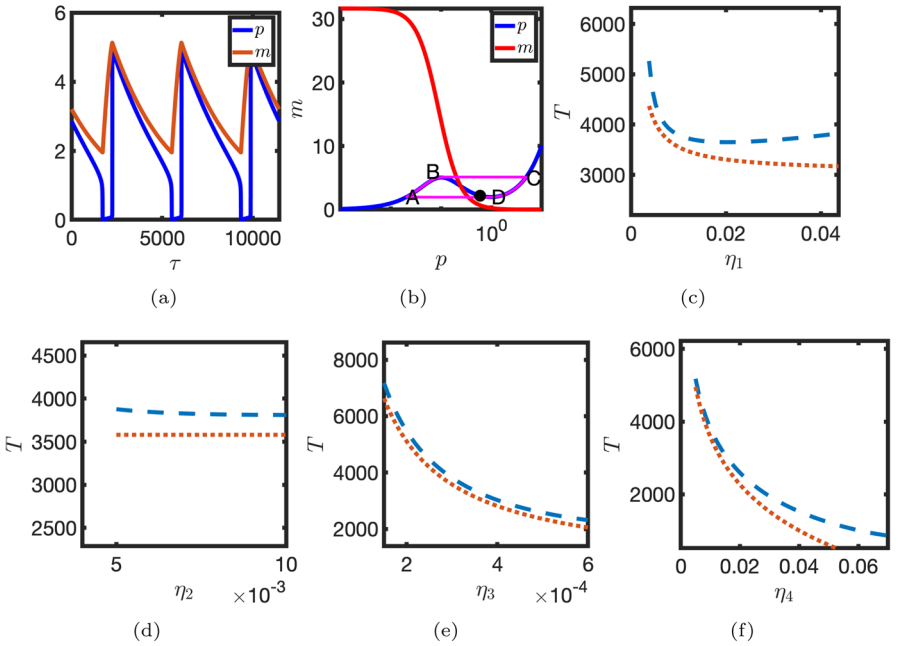

Fig. 5 Estimation of the oscillator period in the relaxation oscillator limit. **a** m and p are plotted against time, τ. **b** Phase plane trajectory. p nullcline (blue line). m nullcline (red line). Solution trajectory (solid magenta line). **c–f** The approximate oscillator period, T, is plotted against **c** η_1, **d** η_2, **e** η_3 and **f** η_4. Numerical estimates (dashed lines) were obtained by solving Eq. (2) numerically. Dotted lines [Eq. (17)]. $\eta_1 = 0.009$, $\eta_3 = 0.0003$. Other parameter values as in Table 1 (Color figure online)

parameter η_4, condition (13) can be approximated by

$$\frac{k_2}{k_5} < 1 - 4\sqrt{\frac{X_0}{\alpha} + \frac{k_3}{k_4}}. \tag{18}$$

These conditions imply the more restrictive bounds

$$\frac{\alpha}{X_0} > 16 \quad \text{and} \quad \frac{k_4}{k_3} > 16.$$

A region of parameter space in which oscillations are possible is depicted in Fig. 6. The results imply that an experimental perturbation that independently either: (i) decreases the translation rate ratio; (ii) decreases the steady state level of X; or (iii) decreases mRNA stability relative to protein stability could be sufficient to move the system out of the oscillatory regime. Moreover, mRNA must be more stable the protein in order for oscillatory solutions to be possible.

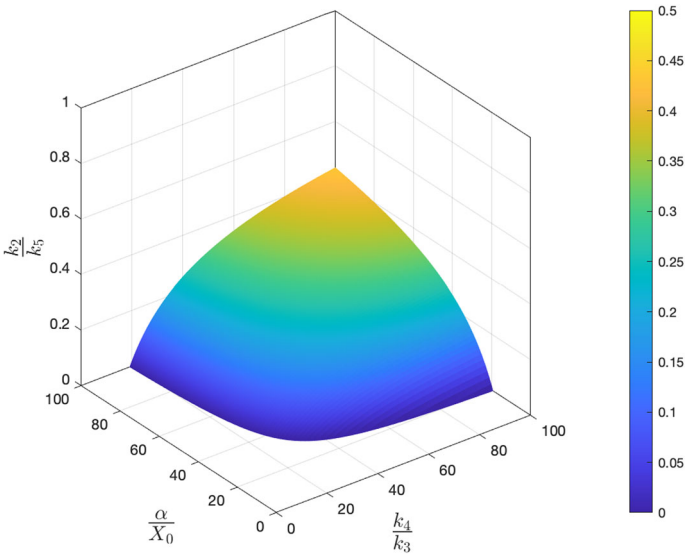

Fig. 6 Necessary conditions for instability of the unique steady state. Values of k_2/k_5 below which instability is possible are plotted against k_4/k_3 and α/X_0 [see Eq. (18)] (Color figure online)

Upon redimensionalising Eq. (17), an estimate for the oscillator period in the relaxation oscillator limit is given by

$$T = \frac{k_5 P_0}{2k_1 k_4 \sqrt{1 + \frac{\alpha}{X_0}\frac{k_3}{k_4}}} \frac{\alpha}{X_0} + \frac{1}{k_2} \ln\left(\frac{\sqrt{\frac{k_4}{k_3}}\sqrt{\frac{\alpha}{X_0}}}{4\sqrt{\frac{k_4}{k_3} + \frac{\alpha}{X_0}}} \right).$$

Notably, whilst the oscillator period increases linearly with the mRNA half-life ($\ln 2/k_2$), it has an inverse dependence on the protein half life ($\ln 2/k_5$). It is also inversely dependent on the transcription rate, k_1, and there is a strong nonlinear dependence on translation rates (k_3 and k_4). The dimensional protein and mRNA oscillator amplitudes are given at leading order in the relaxation oscillator limit by

$$A_P = \frac{P_0}{2}\frac{\alpha}{X_0}\left(\frac{1}{1 + \frac{\alpha}{X_0}\frac{k_3}{k_4}}\right)^{\frac{1}{2}} \quad \text{and} \quad A_M = \frac{P_0}{2}\frac{k_5}{k_4}\frac{\alpha}{X_0}\left(\frac{1}{1 + \frac{\alpha}{X_0}\frac{k_3}{k_4}}\right)^{\frac{1}{2}},$$

respectively. Notably, the amplitude of protein and mRNA oscillations are independent of mRNA production and degradation rates. Moreover, the ratio of protein to mRNA amplitudes can be approximated by

$$\frac{A_P}{A_M} = \frac{k_4}{k_5}.$$

7 Discussion

A model of the Notch signalling pathway was recently developed in which it was assumed that an intermediate factor that is under the same transcriptional regulation as Hes/Her genes inhibits the translation rate of transcribed mRNA (Murray et al. 2021). Numerical simulations were previously used to explore model behaviour and a number of experimentally testable hypotheses were defined. However, qualitative analysis of the proposed model is required in order to better characterise its behaviours and allow it to be applied in other contexts.

In this study the previous model was nondimensionalised. It was shown that the p nullcline had biologically relevant extrema if the parameter η_4 is sufficiently small. The biological interpretation of this result is that for nontrivial behaviours levels of X must be sufficiently high so as to significantly downregulate the translation rate. In order that model parameters are biologically relevant it was also found that $\eta_2 < \eta_4$, i.e. the effective IC50 for transcriptional repression is an order of magnitude smaller than the IC50 for the switch of translation from low to high rates.

After performing a steady state analysis, it was shown that the model possesses a unique steady state for biologically relevant parameter values. Linear stability analysis demonstrated that the unique steady state was linearly stable when the intersection of the nullclines occurs on either the left- or right-most branches of the p nullcline. In the case where the steady state arises on the middle branch of the p nullcline, it is conditionally stable. If the mRNA is more stable than the protein ($\eta_3 < 1$) one can always identify an interval of the parameter η_1 such that the unique steady state is unstable. Upon application of the Poincare Bendixson theorem, there is therefore always a range of η_1 that yields oscillatory solutions given (provided η_3, η_4 and η_2 are sufficiently small).

Application of numerical continuation confirmed that there is a minimal value of the parameter η_3 below which oscillatory solutions can be found. Moreover, as η_1 increases from below there is Hopf bifurcation that is either subcritical or supercritical. Notably, a previous study of isolated zebrafish PSM cells has postulated a Stuart Landau model which has a supercritical Hopf bifurcation, behaviour that is consistent with the proposed model (Webb et al. 2016).

In the limit where the rate constants associated with mRNA (η_1 and η_3) are chosen to be relatively small, the model behaves like a relaxation oscillator. In this case the period is approximated by assuming that the trajectory is in quasi-equilibrium on the left- and right branches of the p nullcline. Close to the local maximum of the p nullcline dynamics are relatively slow and an extra term must be accounted for that describes the time taken for protein levels to increase sufficiently so as to upregulate the translation rate.

The dimensionless equations (2) have previously been proposed as an illustrative model that describes how coupled positive and negative feedback loops give rise to 'frustrated bistability' (Krishna et al. 2009). The analysis performed heres generalises the work of Krishna et al. (2009) by considering dependence of model behaviour on the parameter η_4 as well as deriving explicit formulae for the oscillator period and bounds for the domain of oscillatory solutions. Moreover, the derivation of the model in this study differs from that of Krishna et al. (2009); here we consider regulation

of the transcriptional and translational products of a single gene whilst Krishna et al. (2009) consider a model for protein-protein interaction.

The role of Notch signalling in regulating the period of the segmentation clock oscillator appear to be species dependent. In the zebrafish embryo it has been shown that levels of Notch signalling are anticorrelated with the oscillator period. When Notch signalling is increased via overexpression of Delta ligand the period decreases (Liao et al. 2016). Moreover, when levels of Notch signalling are reduced via gamma secretase treatment the period of the segmentation clock increases (Herrgen et al. 2010). In contrast, when mouse and chicken embryos are pharmaceutically treated with compounds that increase levels of the Notch intracellular domain, the period of the segmentation clock is increased (Wiedermann et al. 2015). In the proposed model intercellular coupling is not explicitly accounted for. Rather, the parameter k_1 (and hence η_1) can act as a proxy for levels of Notch signalling (assuming that levels of NICD regulate the maximal transcription rate). In this study it has been shown that the oscillator period can either increase or decrease with η_1. Thus the proposed model supports the hypothesis that species-specific differences in rate constants could explain the contrasting observation of the dependence of oscillator period on levels of Notch signalling.

It is notable that oscillatory solutions of the model are permitted only if mRNA is more stable than protein. Whilst in mouse fibroblasts mRNAs have been measured to be on average approximately fives times less stable than the protein that they encode, this is not true for approximately 10% of mRNAs (Schwanhäusser et al. 2011). Gene ontology analysis associates genes that encode relatively stable mRNAs with biological processes such as tissue morphogenesis, cell proliferation, phosphorylation and positive regulation of signal transduction (Schwanhäusser et al. 2011). Moreover, direct measurement of Hes1 mRNA and protein in mouse PSM tissue yielded half lives of 24.1 and 22.3 min, respectively (Hirata et al. 2002). Additionally, in zebrafish the half life of Her7 protein has been measured to be to 3.5 min at 24° and it has been inferred using simulations that the mRNA half life is between 2 and 6 min (Ay et al. 2013). Together, these measurements suggest that Hes1/Her7 genes encode mRNA and proteins that have similar half lives.

The relaxation oscillator analysis yields a number of experimentally testable predictions. For example, a decrease in the parameter k_5 (i.e. more stable protein) would result in a smaller oscillatory period and an increase in the amplitude of protein oscillation relative to that of the mRNA. In contrast, a decrease in parameter k_2 (i.e. making the mRNA more stable) would result in a larger period of oscillation but with an unchanged oscillation amplitude. These predictions allow for the proposed model to be distinguished from delayed negative feedback models where the oscillator period is predicted to increase linearly with both the protein and mRNA half lives Lewis (2003).

In this study a qualitative analysis has been performed on a model of a gene regulatory network in which translation as well as transcription rates are regulated by the product of a pathway. The main finding is that oscillatory solutions are possible only when: the regulation of translation rate is sufficiently large and mRNA is sufficiently more stable than protein. The qualitative analysis allows for the previous model to be applied in different biological contexts.

Appendix A Nullclines

For small p the asymptote of the p nullcline is given by the line $m = p/\eta_4$ whilst for large p it is given by the line $m = p$. To identify turning points of the p nullcline $m_2(p)$, Eq. (4) is differentiated with respect to p and the equation

$$\frac{\mathrm{d}\bar{m}_2}{\mathrm{d}p} = \frac{p^4 + p^2(3\eta_4 - 1) + \eta_4}{(\eta_4 + p^2)^2} = 0, \tag{19}$$

is solved. Turning points thus occur at

$$p_c = \pm\left(\frac{1 - 3\eta_4 \pm \sqrt{(1 - 9\eta_4)(1 - \eta_4)}}{2}\right)^{\frac{1}{2}}. \tag{20}$$

A necessary condition for unique real turning points is that

$$(1 - 9\eta_4)(1 - \eta_4) > 0,$$

an inequality that is satisfied in the intervals

$$\eta_4 < \frac{1}{9} \quad \text{and} \quad \eta_4 > 1.$$

For $p_c \in \Re^+$, a further requirement is that

$$\eta_4 < \frac{1}{3}.$$

Hence there are two unique real positive turning points if

$$\eta_4 < \frac{1}{9}.$$

A.1 An Approximation for the Turning Points of the *p* Nullcline

Given that $\eta_4 < 1/9$ then, upon applying the binomial expansion to Eq. (20), the local maximum and minimum are approximated by

$$(p_1, m_1) = \left(\sqrt{\eta_4}(1 + 2\eta_4 + O(\eta_4^2)), \frac{1}{2\sqrt{\eta_4}}\left(1 + \eta_4 + O(\eta_4^2)\right)\right),$$

and

$$(p_2, m_2) = (1 - 2\eta_4 + O(\eta_4^2), 2 - 2\eta_4 + O(\eta_4^2)),$$

respectively. Note that (p_1, m_1) is a local maximum and (p_2, m_2) a local minimum of the p nullcline.

A.2 Parameter Constraints in the Case of a Non Monotonic *p* Nullcline

Consider the definitions of η_2 and η_4 given in Eq. (3). The parameter ratio $\frac{k_4}{k_3}$ can be expressed in terms of dimensionless parameters in the form

$$\frac{k_4}{k_3} = \frac{1 - \eta_4}{\eta_4 - \eta_2}. \tag{21}$$

Hence in the case $\eta_4 < 1$, the assumption that the parameters k_3 and k_4 are positive implies that

$$\eta_2 < \eta_4.$$

Moreover, the constraints $\eta_2 < \eta_4 < 1/9$ imply that

$$\frac{k_4}{k_3} > 8.$$

Hence the translation rate that is nonlinearly regulated must be significantly larger than the background rate k_3 in order for the p nullcline to be non-monotonic. Furthermore, using the definition of η_2 in Eq. (3) together with the constraint $\eta_2 < \eta_4 < 1/9$ implies that

$$\frac{\alpha}{X_0} > 8.$$

Recall that the quasi steady state approximation for X yields

$$X = \frac{\frac{\alpha}{X_0}}{1 + \left(\frac{P}{P_0}\right)^2}.$$

Hence for the p nullcline to be non-monotonic, X must be sufficiently large in magnitude such that it can have a a strong effect on the net translation rate.

Appendix B Steady State Analysis

Suppose that (p^*, m^*) is a steady state solution of equations (2). p^* satisfies the fifth order polynomial

$$h(p^*) = p^{*5} + p^{*3}(\eta_2 + 1) - p^{*2}\frac{\eta_1\eta_2}{\eta_3} + \eta_2 p^* - \frac{\eta_1\eta_2\eta_4}{\eta_3} = 0. \tag{22}$$

The m nullcline [Eq. (5)] is bounded above by $m = \eta_1/\eta_3$. Hence $m^* < \eta_1/\eta_3$. The p nullcline [Eq. (4)] is bounded below by the line $m = p\,\forall p > 0$. Hence $m^* > p^*$ and therefore

$$p^* \in [0, \eta_1/\eta_3].$$

Consider the steady state Eq. (22). Define

$$g_1(p^*) = p^{*2}\left(p^{*3} + p^*(1 + \eta_2) - \frac{\eta_1\eta_2}{\eta_3}\right), \tag{23}$$

and

$$g_2(p^*) = \eta_2\left(\frac{\eta_1\eta_4}{\eta_3} - p^*\right), \tag{24}$$

such that Eq. (6) can be expressed as $g_1(p^*) = g_2(p^*)$.

The function $g_2(p^*)$ is linear in p^* with the intercept at

$$g_2(0) = \frac{\eta_2\eta_1\eta_4}{\eta_3},$$

and root at

$$p^* = \frac{\eta_1\eta_4}{\eta_3}.$$

$g_1(p^*)$ is a fifth order polynomial. Note that

$$g_1(0) = 0, \quad g_1'(0) = 0 \quad \text{and} \quad g_1''(0) < 0.$$

As the leading order term at $p^* = 0$ is negative and $g_1 \to \infty$ as $p^* \to \infty$, g_1 has at least one real positive root. Moreover, applying Descartes' rule of signs, g_1 has at most one real positive root. Hence g_1 has a unique real positive root at $p^* = \delta \in [0, \eta_1/\eta_3]$.

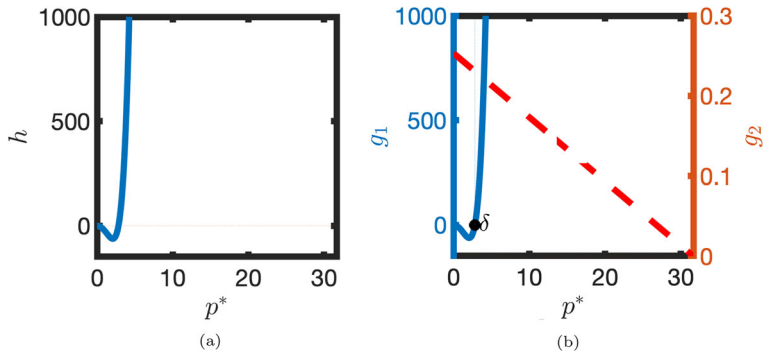

Fig. 7 **a** h [Eq. (6)] is plotted against p^*. **b** g_1 [Eq. (23), solid blue line] and g_2 [Eq. (24), dashed red line] are plotted against p^* (Color figure online)

Turning points of g_1 satisfy

$$g_1' = 5p^{*4} + 3p^{*2}(1+\eta_2) - 2p^*\frac{\eta_1\eta_2}{\eta_3} = 0$$

Application of Descartes rule of signs implies that g_1 has at most one turning point for $p^* > 0$. Hence in the interval $p^* \in [0, \delta]$, $g_1 < 0$ and g_1 has a unique turning point (see Fig. 7).

Consider the interval $[0, \delta]$. As $g_1 < 0$ and $g_2 > 0$, the steady state solution p^* does not lie in the interval $[0, \delta]$.

Now consider the interval $\left[\delta, \frac{\eta_1}{\eta_3}\right]$. At η_1/η_3

$$g_1\left(\frac{\eta_1}{\eta_3}\right) > 0,$$

and

$$g_2\left(\frac{\eta_1}{\eta_3}\right) = 0.$$

Hence

$$g_1\left(\frac{\eta_1}{\eta_3}\right) > g_2\left(\frac{\eta_1}{\eta_3}\right).$$

At $p^* = \delta$, $g_1(\delta) = 0$ and $g_2(\delta) > 0$. Thus

$$g_1(\delta) < g_2(\delta).$$

As in the interval $\left[\delta, \frac{\eta_1}{\eta_3}\right]$

$$g_2'(p^*) < 0$$

and

$$g_1'(p^*) > 0,$$

there is one intersection $\gamma \in \left[\delta, \frac{\eta_1}{\eta_3}\right]$. Hence Eq. (22) has a unique steady state in $[\delta, \eta_1/\eta_3]$.

B.1 p^* is a Monotonically Increasing Function of η_1

Differentiating Eq. (6) with respect to η_1 yields

$$\frac{dp^*}{d\eta_1} = \frac{\frac{\eta_2}{\eta_3}(p^{*2} + \eta_4)}{5p^{*4} + 3p^{*2}(1+\eta_2) - 2p^*\frac{\eta_1\eta_2}{\eta_3} + \eta_2}.$$

As the numerator is positive, the derivative is positive if the condition

$$5p^{*4} + 3p^{*2}(1+\eta_2) - 2p^*\frac{\eta_1\eta_2}{\eta_3} + \eta_2 > 0$$

holds for any p^* that is a solution of Eq. (22). This inequality holds in the case of a unique bounded solution to the steady state problem.

In the case where $\eta_2 < 1/9$ this inequality is satisfied for $p^* > \frac{2}{27}\frac{\eta_1}{\eta_3}$. Hence the inequality is satisfied for all $p^* \in [0, \eta_1/\eta_3]$. Hence p^* is an increasing function of the parameter η_1.

Appendix C Linear stability analysis

Positivity of the determinant of the Jacobian matrix requires

$$-\eta_3(m^* f'(p^*) - 1) + \frac{2p\eta_1}{\eta_2}\frac{f(p^*)}{(1+\frac{p^*}{\eta_2})^2} > 0,$$

where

$$f(p^*) = \frac{\eta_4 + p^{*2}}{1 + p^{*2}}.$$

Substituting for

$$m^* = \frac{\frac{\eta_1}{\eta_3}}{\left(1 + \frac{p^{*2}}{\eta_2}\right)},$$

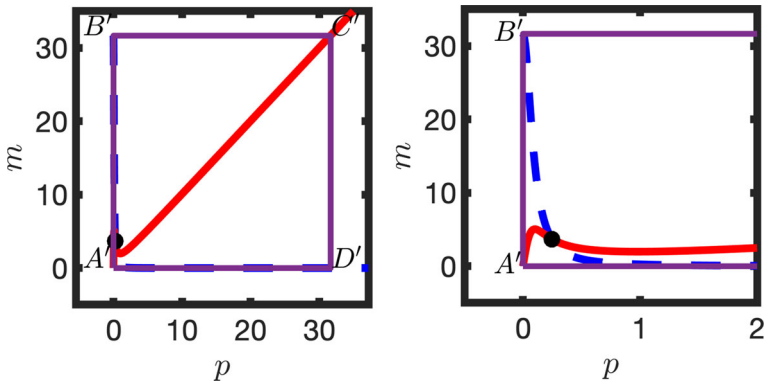

Fig. 8 **a** A confined set is depicted in the mp phase plane. p nullcline (solid red line) m nullcline (dashed blue line). The confined set is given by $A'B'C'D'A'$. **b** Inset for **a** (Color figure online)

yields, after rearrangement and simplification,

$$p^{*4} + \eta_4 p^{*2} + (\eta_4 - \eta_2) > 0.$$

Noting that

$$\eta_2 < \eta_4,$$

the inequality is therefore satisfied $\forall p > 0$. Hence the Jacobian determinant is positive definite.

Appendix D Poincare Bendixson

A confined set of Eq. (2) is given by A′B′D′C′A′ (see Fig. 8). Let A' represent the origin and B′ represent the point $(0, \eta_1/\eta_3)$. The outward unit normal on A'B' is $\mathbf{n}_{A'B'} = [-1, 0]$. On this line segment

$$\mathbf{n}_{A'B'} \cdot \left[\frac{dp}{d\tau}, \frac{dm}{d\tau}\right] = -\frac{dp}{d\tau} < 0.$$

Let C′ represent the point $(p^{\dagger}, \eta_1/\eta_3)$ such that

$$\frac{p^{\dagger}(1 + p^{\dagger 2})}{\eta_4 + p^{\dagger 2}} = \frac{\eta_1}{\eta_3}.$$

$p^\dagger$ is uniquely defined so long as $\eta_1/\eta_3 > m_1$. The outward unit normal on B′C′ is $\mathbf{n}_{B'C'} = [0, 1]$. On B′C′

$$\mathbf{n}_{B'C'} \cdot \left[\frac{dp}{d\tau}, \frac{dm}{d\tau}\right] = -\frac{dm}{d\tau} < 0.$$

Let D′ represent $(p^\dagger, 0)$. The outward unit normal on C'D' is $\mathbf{n}_{C'D'} = [1, 0]$. On C'D'

$$\mathbf{n}_{C'D'} \cdot \left[\frac{dp}{d\tau}, \frac{dm}{d\tau}\right] = -\frac{dp}{d\tau} < 0.$$

Finally, on D'A' the outward unit normal is $\mathbf{n}_{D'A'} = [0, -1]$. On D'A'

$$\mathbf{n}_{D'A'} \cdot \left[\frac{dp}{d\tau}, \frac{dm}{d\tau}\right] = -\frac{dm}{d\tau} < 0.$$

Hence A′B′C′D′A′ defines a confined set. Therefore, by the Poincare Bendixson theorem, when the unique steady state is linearly unstable, the solution is a stable limit cycle.

Appendix E Period estimate

Let

$$\eta_1 = \epsilon\hat{\eta}_1 \quad \text{and} \quad \eta_3 = \epsilon\hat{\eta}_3,$$

where

$$\epsilon \ll \sqrt{\eta_4} < \frac{1}{9}.$$

Equations (2) transform to

$$\begin{aligned} \frac{\mathrm{d}m}{\mathrm{d}\tau} &= \epsilon\left(\frac{\hat{\eta}_1}{1+\frac{p^2}{\eta_2}} - \hat{\eta}_3 m\right), \\ \frac{\mathrm{d}p}{\mathrm{d}\tau} &= m\frac{(\eta_4 + p^2)}{1+p^2} - p, \end{aligned} \tag{25}$$

and an oscillatory solution can be approximated using a slow-fast timescale analysis.

Consider the trajectory ABCDA with coordinates

$$(m_A, p_A) = (2 - 2\eta_4, 2\eta_4), \quad (m_B, p_B) = \left(\frac{1}{2\sqrt{\eta_4}}(1+\eta_4), \sqrt{\eta_4}(1+2\eta_4)\right),$$

$$(m_C, p_C) = \left(\frac{1}{2\sqrt{\eta_4}}(1+\eta_4), \frac{1}{2\sqrt{\eta_4}}(1+\eta_4)\right) \quad \text{and} \quad (m_D, p_D) = (2-2\eta_4, 1-2\eta_4). \tag{26}$$

On the segment AB p is assumed to be in quasi-equilibrium, i.e.

$$m = \frac{p(1+p^2)}{\eta_4 + p^2}$$

and the ODE

$$\frac{\mathrm{d}p}{\mathrm{d}\tau} = \frac{dp}{dm}\frac{dm}{d\tau} = \epsilon \frac{(\eta_4+p^2)^2}{p^4 + p^2(3\eta_4 - 1) + \eta_4}\left(\frac{\hat{\eta}_1}{1+\frac{p^2}{\eta_2}} - \hat{\eta}_3 \frac{p(1+p^2)}{\eta_4+p^2}\right).$$

is integrated from p_A to p_B. After applying separation of variables the time spent on the segment AB is

$$T_{AB} = \frac{1}{\epsilon}\int_{p_A}^{p_B} \frac{\frac{dm}{dp}}{\frac{dm}{d\tau}} dp = \frac{1}{\epsilon}\int_{p_A}^{p_B} \frac{p^4 + p^2(3\eta_4 - 1) + \eta_4}{(\eta_4+p^2)^2\left(\frac{\hat{\eta}_1}{1+\frac{p^2}{\eta_2}} - \hat{\eta}_3\frac{p(1+p^2)}{\eta_4+p^2}\right)} dp. \tag{27}$$

The integral in Eq. (27) is approximated as follows. As the term

$$g(p) = \left(\frac{\hat{\eta}_1}{1+\frac{p^2}{\eta_2}} - \hat{\eta}_3\frac{p(1+p^2)}{\eta_4+p^2}\right)$$

is a decreasing function of p for $p \in [p_A, p_B]$ it is bounded in the interval $[g(p_B), g(p_A)]$.

Hence

$$\begin{aligned} & T_{AB} \in \left[\frac{1}{g(p_A)}, \frac{1}{g(p_B)}\right]\frac{1}{\epsilon}\int_{m_A}^{m_B} dm \\ \implies & T_{AB} \in \frac{1}{\epsilon}\left[\frac{1}{g(p_A)}, \frac{1}{g(p_B)}\right]\left(\frac{1}{2\sqrt{\eta_4}} - 2 + \frac{\sqrt{\eta_4}}{2} + 2\eta_4 + O(\eta_4^{\frac{3}{2}})\right). \end{aligned} \tag{28}$$

At point B

$$\frac{dm}{d\tau} \sim O(\epsilon) \quad \text{and} \quad \frac{dp}{d\tau} \sim O(\sqrt{\eta_4}).$$

Given that $\epsilon \ll \sqrt{\eta_4}$, on the segment BC m is a slow variable, approximated by

$$m \sim m_B,$$

and p rapidly increases until the trajectory reaches the point C on the right branch of the p nullcline.

On the segment CD, p is assumed to be in quasi-steady state. As $p > 1 \gg \eta_2$, the m dynamics are approximated by

$$\frac{\mathrm{d}m}{\mathrm{d}\tau} = -\eta_3 m.$$

Thus the time spent on the segment CD is

$$T_{CD} = \frac{1}{\epsilon \hat{\eta}_3} \ln\left(\frac{m_C}{m_D}\right).$$

On the segment DA, dynamics are fast. m is is approximated by

$$m = M_D$$

and

$$\frac{\mathrm{d}p}{\mathrm{d}\tau} = O(1).$$

Thus the period is approximately given by

$$T = T_{AB} + T_{CD}. \tag{29}$$

Considering the upper bound $g = g(p_A)$ yields the estimate

$$T_{AB} = \frac{1}{\epsilon}\left(\frac{1}{g(p_A)}\left(\frac{1}{2\sqrt{\eta_4}} - 2 + \frac{\sqrt{\eta_4}}{2} + 2\eta_4 + O(\eta_4^{\frac{3}{2}})\right)\right).$$

Hence the period is approximated by

$$T = \frac{1}{\epsilon}\left(\frac{1}{g(p_A)}\left(\frac{1}{2\sqrt{\eta_4}} - 2 + \frac{\sqrt{\eta_4}}{2} + 2\eta_4 + O(\eta_4^{\frac{3}{2}})\right) + \frac{1}{\hat{\eta}_3}\ln\left(\frac{1}{4\sqrt{\eta_4}}\frac{1+\eta_4}{(1-\eta_4)}\right)\right). \tag{30}$$

Finally, it is noted that $g < \eta_1$. For simplicity g is represented by the upper bound η_1. Considering leading order in η_4 yields Eq. (17).

At the local maximum of the p nullcline $dp/d\tau$ is $O(\sqrt{\eta_4})$. Hence for $\epsilon \sim \sqrt{\eta_4}$ the fast-slow analysis will become inaccurate. The time for p to increase from the local maximum of the p nullcline ($p = \sqrt{\eta_4}$) to the IC50 for the translation switch is approximately

$$T_{BB'} = \frac{1}{2\sqrt{\eta_4}} - 1$$

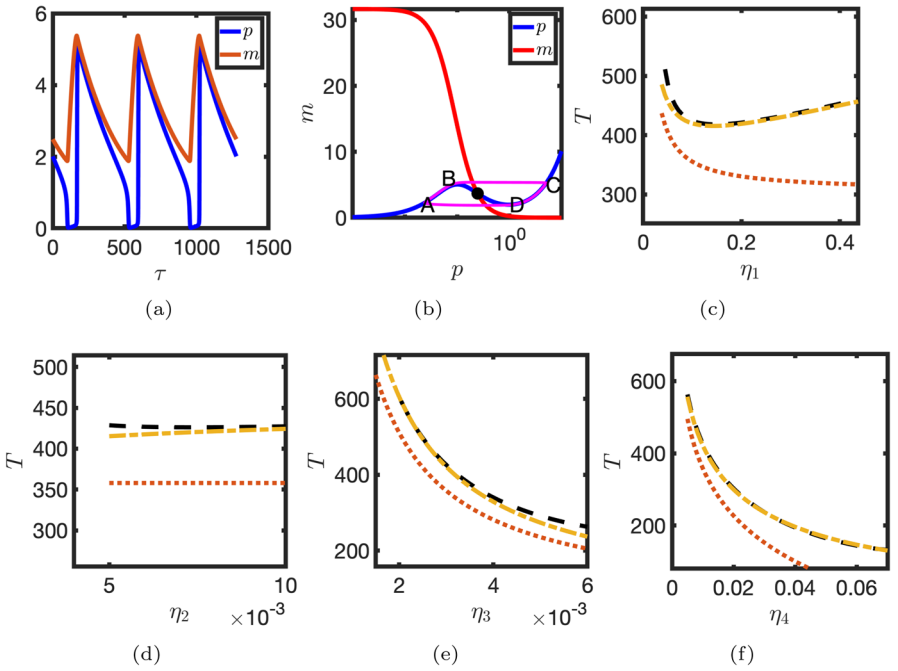

Fig. 9 Estimation of the oscillator period in the relaxation oscillator limit. $\eta_1 = 0.09$, $\eta_3 = 0.003$. (c-f) Dot-dashed line [Eq. (31)]. Other details as in Fig. 5 (Color figure online)

Linearising about the local maximum of the p nullcline, m increases by amount

$$\Delta m = \epsilon \left(\frac{\hat{\eta}_1}{1 + \frac{\eta_4}{\eta_2}} - \hat{\eta}_3 \frac{1}{2\sqrt{\eta_4}} \right) T_{BB'}$$

in time $T_{BB'}$. On the descent this increase in m requires an additional time

$$T_{B'C} = \frac{1}{\eta_3} \ln \left(1 + \frac{\Delta m}{m_C} \right).$$

Thus the period is approximately given by

$$T = T_{AB} + T_{BB'} + T_{B'C} + T_{CD}. \tag{31}$$

In Fig. 9 the derived estimates for the oscillator period are compared with numerical estimates. In this case $\eta_1 \sim O(\sqrt{\eta_4})$. Note that the dependence of oscillator period on η_1 is no longer monotonic. For small η_1 the period increases as η_1 decreases as a result of the progression of the solution along AB (transcription is a limiting step). However, for larger η_1 the period increases with η_1. This effect is due to the overshoot at the local maximum of the p nullcline.

References

Allenspach EJ, Maillard I, Aster JC, Pear WS (2002) Notch signaling in cancer. Cancer Biol Ther 1(5):466–476

Alon U (2019) An introduction to systems biology: design principles of biological circuits. CRC Press

Ay A, Knierer S, Sperlea A, Holland J, Özbudak EM (2013) Short-lived her proteins drive robust synchronized oscillations in the zebrafish segmentation clock. Development 140(15):3244–3253

Bone RA, Bailey CS, Wiedermann G, Ferjentsik Z, Appleton PL, Murray PJ, Maroto M, Dale JK (2014) Spatiotemporal oscillations of Notch1, Dll1 and NICD are coordinated across the mouse PSM. Development 141(24):4806–4816

Bonev B, Stanley P, Papalopulu N (2012) MicroRNA-9 modulates Hes1 ultradian oscillations by forming a double-negative feedback loop. Cell Rep 2(1):10–18

Chaplain M, Ptashnyk M, Sturrock M (2015) Hopf bifurcation in a gene regulatory network model: Molecular movement causes oscillations. Math Models Methods Appl Sci 25(06):1179–1215

Dankowicz H, Schilder F (2013) Recipes for continuation. SIAM, Philadelphia

Geva-Zatorsky N, Rosenfeld N, Itzkovitz S, Milo R, Sigal A, Dekel E, Yarnitzky T, Liron Y, Polak P, Lahav G et al (2006) Oscillations and variability in the p53 system. Mol Syst Biol 2(1):2006–0033

Gonze D, Abou-Jaoudé W (2013) The Goodwin model: behind the hill function. PLoS One 8(8):69573

Goodfellow M, Phillips NE, Manning C, Galla T, Papalopulu N (2014) Microrna input into a neural ultradian oscillator controls emergence and timing of alternative cell states. Nat Commun 5(1):1–10

Herrgen L, Ares S, Morelli LG, Schröter C, Jülicher F, Oates AC (2010) Intercellular coupling regulates the period of the segmentation clock. Curr Biol 20(14):1244–1253

Hirata H, Yoshiura S, Ohtsuka T, Bessho Y, Harada T, Yoshikawa K, Kageyama R (2002) Oscillatory expression of the BHLH factor Hes1 regulated by a negative feedback loop. Science 298(5594):840–843

Hubaud A, Regev I, Mahadevan L, Pourquie O (2017) Excitable dynamics and Yap-dependent mechanical cues drive the segmentation clock. Cell 171(3):668–682

Kageyama R, Ohtsuka T, Kobayashi T (2007) The Hes gene family: repressors and oscillators that orchestrate embryogenesis. Development 134(7):1243–1251

Krishna S, Semsey S, Jensen M (2009) Frustrated bistability as a means to engineer oscillations in biological systems. Phys Biol 6(3):036009

Lewis J (2003) Autoinhibition with transcriptional delay. Curr Biol 13(16):1398–1408

Liao B-K, Jörg DJ, Oates AC (2016) Faster embryonic segmentation through elevated Delta-Notch signalling. Nat Commun 7(1):1–12

Mollen EW, Lent J, Tjan-Heijnen VC et al (2018) Moving breast cancer therapy up a notch. Front Oncol 8:518

Monk NA (2003) Oscillatory expression of Hes1, p53, and NF-κB driven by transcriptional time delays. Curr Biol 13(16):1409–1413

Murray PJ, Ocana E, Meijer HA, Dale JK (2021) Auto-regulation of transcription and translation: oscillations, excitability and intermittency. Biomolecules 11(11):1566

Novák B, Tyson JJ (2008) Design principles of biochemical oscillators. Nat Rev Mol Cell Biol 9(12):981–991

Schwanhäusser B, Busse D, Li N, Dittmar G, Schuchhardt J, Wolf J, Chen W, Selbach M (2011) Global quantification of mammalian gene expression control. Nature 473(7347):337–342

Sel'Kov E (1968) Self-oscillations in glycolysis 1. A simple kinetic model. Eur J Biochem 4(1):79–86

Siebel C, Lendahl U (2017) Notch signaling in development, tissue homeostasis, and disease. Physiol Rev 97(4):1235–1294

Sturrock M, Terry AJ, Xirodimas DP, Thompson AM, Chaplain MA (2011) Spatio-temporal modelling of the Hes1 and p53-Mdm2 intracellular signalling pathways. J Theor Biol 273(1):15–31

Tyson JJ, Novák B (2010) Functional motifs in biochemical reaction networks. Annu Rev Phys Chem 61(1):219–240

van Es JH, Van Gijn ME, Riccio O, Van Den Born M, Vooijs M, Begthel H, Cozijnsen M, Robine S, Winton DJ, Radtke F et al (2005) Notch/γ-secretase inhibition turns proliferative cells in intestinal crypts and adenomas into goblet cells. Nature 435(7044):959–963

Webb AB, Lengyel IM, Jörg DJ, Valentin G, Jülicher F, Morelli LG, Oates AC (2016) Persistence, period and precision of autonomous cellular oscillators from the zebrafish segmentation clock. Elife 5:08438

Wiedermann G, Bone RA, Silva JC, Bjorklund M, Murray PJ, Dale JK (2015) A balance of positive and negative regulators determines the pace of the segmentation clock. eLife 4:e05842
Winfree AT (2001) The geometry of biological time, vol 12. Springer